https://dx.doi.org/10.1016/j.measurement.2017.09.029

Improved Decentralized Structural Identification with Output−only Measurements

Pinghe Ni [1, 2], Yong Xia [2], Jun Li [1,], Hong Hao [1]*

[1]*Centre for Infrastructural Monitoring and Protection, School of Civil and Mechanical Engineering, Curtin University, Kent Street, Bentley, WA 6102, Australia*

[2]*Department of Civil and Environmental Engineering, The Hong Kong Polytechnic University, Hung Hom, Kowloon, Hong Kong*

Abstract: This paper proposes an improved decentralized structural identification approach with output−only measurements. The improved approach can be used for system identification of both linear and nonlinear structures. A large-scale structure is divided into a number of smaller zones according to its finite element configuration. Each zone is dynamically tested in sequence with its own set of sensor placement. The external excitation forces in each zone are identified using the Kalman filter technique. Structural parameters of the whole structure are divided into several subsets and then updated by using the Newton-SOR method. Both the external excitations and structural parameters are iteratively updated until a defined convergence criterion is met. The proposed technique is then applied to two numerical examples: a six floor building and a planar truss structure. The nonlinear system parameters of the building are correctly identified. The unknown excitation force, damage location, and damage severity in the plane truss structure are successfully identified. The effect of measurement noise on the identified results is also studied. An eight floor shear type structure is finally tested in the laboratory. The experimental results further verify the effectiveness and efficiency of the proposed technique in damage identification using output−only measurements.

Keywords: Decentralized structural identification; Damage identification; Model updating; Force identification; Vibration measurements; Nonlinear system

*Corresponding Author, Centre for Infrastructural Monitoring and Protection, School of Civil and Mechanical Engineering, Curtin University, Kent Street, Bentley, WA 6102, Australia. Email: junli@curtin.edu.au; LI.Jun@connect.polyu.hk, Tel.: +61 8 9266 5140; Fax: +61 8 9266 2681.

1. Introduction

Numerous efforts have been made to develop structural identification methods with unknown input to satisfy the general practical application requirement in field because the input excitation is difficult to be measured under operational conditions of civil structures. When only the output structural responses are available, the corresponding methodologies are usually referred to as output only techniques. Most techniques of this kind identify both the structural parameters and excitation forces simultaneously or successively via an iterative manner. Li and Chen [1] proposed a statistical algorithm to identify the structural parameters and the input information sequentially. Lu and Law [2] proposed a two-stage method based on the dynamic response sensitivity to identify both the structural parameters and excitation forces. Other methods based on Quadratic Sum-Squares Error [3], Sequential nonlinear least-square estimation [4], Extended Kalman Filter [5], etc. have also been reported to conduct the damage identification with unknown input.

Many structural identification techniques are based on the assumption that the structure behaves linearly [6-8]. However, structural failures or damage generally cause nonlinearity to some extent, and therefore damage detection for structures with nonlinear behavior should be considered. Kalman filter technique is one of the most promising methods for nonlinear structural identification. Lei et al. [6] proposed a Kalman filter technique for the identification of nonlinear restoring force with limited input and output measurements. The algorithm sequentially applied the classical Kalman estimator for estimating the structural responses and the recursive least squares estimation for identifying the nonlinear restoring force and unmeasured excitations. Wu and Smyth [7] proposed a damage detection method based on unscented Kalman filter to identify the hysteretic differential models with degradation and pinching. Xie and Feng [8] proposed an iterative unscented Kalman filter for nonlinear structural identification.

The conventional system identification and damage detection methods at the structural element level may be well suitable for small to medium-size structures, but not necessarily suitable for large-scale structures with a large number of structural parameters because a large amount of data is required. In addition, the system identification is generally an inverse problem, which needs a number of iterations and is computationally intensive. The capital cost for sensor installation, practical problems associated with power supply, and the data processing capability of hardware are several typical adverse factors for a high density sensor configuration. Therefore efficient damage detection and model updating with less numbers of sensors is of emerging interest.

Substructural analysis and identification approaches have been proved to be effective and efficient for large scale structures. Weng et al. [9] proposed an inverse substructure-based finite

element model updating technique in the frequency domain. The modal data measured on the global structure are disassembled to substructural flexibility matrices, under the force and displacement compatibility constraints. The substructural eigenparameters can be used to identify local damages, which are more sensitive than the global eigenparameters [10]. Several researchers have developed substructure-based system identification techniques in the time domain. Koh et al. [11] proposed a "divide-and-conquer" damage detection method and the substructural parameters were identified using a genetic algorithm. Yuen and Katafygiotis [12] proposed a substructural identification method based on Bayesian inference. The method calculated the probability distribution of the parameters for identification. Not only the best estimates of the parameters but also their uncertainties can be qualified. Law et al. [13] performed structural damage detection from coupling forces between substructures. Lei et al. [14] proposed a substructural identification method based on the extended Kalman filter. The large-scale structure is divided into several small substructures, and the interface effect from adjacent substructures is treated as unknown input forces. The interface forces of each substructure are identified using the extended Kalman estimator and least-squares estimation.

Time domain substructural identification methods usually have two limitations: (1) the measurements of the interface forces should be available; and (2) the number of sensors should be equal to or larger than the number of interface forces. Several methods have been developed to deal with the first limitation. Koh et al. [15] eliminated the requirement of interface forces using different sets of measurements of the substructure under the same dynamic excitation and thus the interface measurement was not necessary. Li and Law [16] proposed a wavelet based transmissibility matrix for substructural damage identification, where the dynamic responses at one set of degrees-of-freedom (DOFs) of the target substructure were reconstructed from another set of measurement responses. The local damages were identified from minimizing the differences between the measured and the reconstructed sets of responses. Consequently the interface measurements are not required. However, this method is still subject to the second limitation, that is, it requires the number of sensors to be equal to or larger than the number of interface forces [17].

The decentralized method is an alternative solution to the large-scale system identification, which shares the similar idea “divide –and-conquer” of the above-mentioned substructural approaches. Decentralized methods have a significant advantage when used for the full scale model updating. It could conquer the abovementioned two limitations that the substructural methods may suffer from,

to have a good estimation of the pseudo-inverse in the identification by formulating the global optimization as a set of smaller size optimization problems. Decentralized methods have been used for modal identification. Sim et al. [18] proposed a decentralized modal analysis using a decentralized topology in smart wireless sensor networks. The proposed approach consisted of two main steps: the first is the local feature extraction using Eigensystem Realization Algorithm (ERA) or Natural Excitation Technique (NExT) and the other is the global modal property determination using the aggregated local properties in the base station. Another decentralized modal identification method was proposed by Jo et al. [19]. This method was embedded into Imote2 wireless sensor platforms for wireless structural health monitoring. The efficiency of the decentralized modal identification using high-sensitivity sensors was experimentally verified using a steel truss structure. Decentralized methods were also proposed for structural damage identification. Wu et al. [20] proposed a parametric damage detection method based on neural networks. Yun et al. [21] proposed a decentralized damage identification method based on wavelet signal analysis tools. The discrete wavelet coefficients of acceleration were used for damage identification with wavelet entropy indices.

This paper proposes an improved decentralized structural identification technique for both linear and nonlinear structures, by extending the authors' pervious work [22] on damage identification of linear structures only. The significant improvement to further develop the decentralized approach for nonlinear structural identification in this study. The proposed approach combines the Kalman filter technique for force identification and the Newton-SOR method for damage identification. It owns the advantages of both the decentralized method and Kalman filter technique, and could be used for both linear and nonlinear structural identification. The basic formulations of the improved decentralized structural identification approach are described in Section 2. In Section 3, numerical simulations and identification results obtained from a nonlinear system and a planar truss structure are presented and discussed. Experimental studies on an eight-floor building structure are presented in Section 4, followed by the concluding remarks in Section 5.

2. Theoretical Development

Extended and unscented Kalman filter based methods are promising for nonlinear system identification and have been intensively studied [5-8]. In the extended Kalman filter technique, both

unknown structural parameters and forces are included in the state vector and a large number of unknowns may cause the state space equation unstable. Therefore, the method is only applicable to the system identification of small-scale structures with several unknown parameters. In the present study, the Kalman filter technique is used for the state estimation only and the unknown input forces are identified from the state vector with the optimization method. Since the unknown structural parameters are not included in the state vector, the dimension of the state vector is not large and the force identification can then be achieved even for large scale structures. A sensitivity based method, i.e. Netwon-SOR method, is adopted for the decentralized structural damage identification. The Tikhonov regularization is employed to solve the ill-posed inverse problem and obtain a stable solution.

2.1 Equation of motion of a linear or nonlinear system

The equation of motion of a structure under the external excitation can be written as

$$\boldsymbol{M}\ddot{\boldsymbol{x}}(t)+\boldsymbol{F}_c[\dot{\boldsymbol{x}}(t)]+\boldsymbol{F}_s[\boldsymbol{x}(t),\boldsymbol{\theta}]=\boldsymbol{B}\boldsymbol{f}(t) \tag{1}$$

where M is the $n\times n$ mass matrix, $\boldsymbol{x}(t)=[x_1(t),x_2(t),\cdots x_n(t)]^{\mathrm{T}}$ is the displacement vector, $\boldsymbol{F}_c(\dot{\boldsymbol{x}}(t))$, $\boldsymbol{F}_s(\dot{\boldsymbol{x}}(t),\boldsymbol{\theta})$ and $\boldsymbol{f}(t)$ are the dissipating force vector, the stiffness force vector and the excitation force vector, respectively; $\boldsymbol{B}$ is the mapping matrix relating with the location of the applied forces, and $\boldsymbol{\theta}=[\alpha_1,\alpha_2,\cdots\alpha_{ne}]^T$ is the unknown parameter vector of the structure with the number of elements as *ne*. It should be noted that the structural system could be linear or nonlinear, depending on the definition of the dissipating and stiffness force vectors.

The state vector is defined as

$$\boldsymbol{X}(t)=\begin{bmatrix}\boldsymbol{x}(t)\\ \dot{\boldsymbol{x}}(t)\end{bmatrix} \tag{2}$$

Transforming the equation of motion in Eq. (1) as a state equation, we have

$$\dot{\boldsymbol{X}}(t)=\boldsymbol{J}(\boldsymbol{X}(t),\boldsymbol{\theta},\boldsymbol{f}(t))=\begin{bmatrix}\dot{\boldsymbol{x}}(t)\\ \boldsymbol{M}^{-1}\left(\boldsymbol{B}\boldsymbol{f}(t)-\boldsymbol{F}_c[\dot{\boldsymbol{x}}(t)]-\boldsymbol{F}_s[\boldsymbol{x}(t),\boldsymbol{\theta}]\right)\end{bmatrix} \tag{3}$$

Usually, only a limited number of accelerometers are deployed on structures to measure the vibrational acceleration responses. The measurement vector can be written as

$$\begin{aligned} \boldsymbol{Y}(t) &= \boldsymbol{d}\ddot{\boldsymbol{x}}(t) + \boldsymbol{v}(t) \\ &= \boldsymbol{D}\boldsymbol{f}(t) - \boldsymbol{d}\boldsymbol{M}^{-1}(\boldsymbol{F}_{\mathrm{c}}[\dot{\boldsymbol{x}}(t)] + \boldsymbol{F}_{\mathrm{s}}[\boldsymbol{x}(t),\boldsymbol{\theta}]) + \boldsymbol{v}(t) \end{aligned} \tag{4}$$

where $\boldsymbol{D} = \boldsymbol{d}\boldsymbol{M}^{-1}\boldsymbol{B}$, $\boldsymbol{d}$ is associated with the locations of accelerometers and $\boldsymbol{v}(t)$ is the measurement noise vector assumed to be a Gaussian white noise vector with zero mean and a covariance matrix $E(\boldsymbol{v}_i\boldsymbol{v}_j^T) = \boldsymbol{R}_{ij}\delta_{ij}$, in which δ_{ij} is the Kroneker delta and $\boldsymbol{R}_{ij}$ is the variance matrix of the measurement noises.

Eq. (4) can be further expressed in the discrete form as [5, 23]

$$\boldsymbol{Y}_k = \boldsymbol{h}(\boldsymbol{X}_k,\boldsymbol{\theta}) + \boldsymbol{D}\boldsymbol{f}_k + \boldsymbol{v}_k \tag{5}$$

where $\boldsymbol{h}(\boldsymbol{X}_k,\boldsymbol{\theta}) = -\boldsymbol{d}\boldsymbol{M}^{-1}(\boldsymbol{F}_c[\dot{\boldsymbol{x}}_k] + \boldsymbol{F}_s[\boldsymbol{x}_k,\boldsymbol{\theta}])$ with $\dot{\boldsymbol{x}}_k$ and $\boldsymbol{x}_k$ representing the corresponding discrete values of $\dot{\boldsymbol{x}}(t)$ and $\boldsymbol{x}(t)$ at the time instant $t = k\Delta t$, $\boldsymbol{Y}_k$ is the l-dimensional observation (measured) vector at $t = k\Delta t$ (Δt is the sampling interval time), and $\boldsymbol{X}_k$, $\boldsymbol{f}_k$, and $\boldsymbol{v}_k$ are the corresponding discrete values at time instant $t = k\Delta t$.

Field Code Changed
Field Code Changed
Field Code Changed
Field Code Changed
Field Code Changed
Field Code Changed

2.2 Force identification based on Kalman filter technique

The state vector will be estimated first by using the classic Kalman estimator [6], and the unknown excitations are identified by the least squares estimation. Based on the classic Kalman estimator, the state vector at time $t = (k+1)\Delta t$ can be estimated as follows

$$\hat{\boldsymbol{X}}_{k+1} = \tilde{\boldsymbol{X}}_{k+1} + \boldsymbol{K}_k\left\{\boldsymbol{Y}_k - \boldsymbol{h}(\hat{\boldsymbol{X}}_k,\boldsymbol{\theta}) - \boldsymbol{D}\hat{\boldsymbol{f}}_k\right\} \tag{6}$$

and

$$\tilde{\boldsymbol{X}}_{k+1} = \hat{\boldsymbol{X}}_k + \int_k^{k+1}\boldsymbol{J}(\hat{\boldsymbol{X}}_k,\boldsymbol{\theta},\hat{\boldsymbol{f}}_k)dt \tag{7}$$

where $\hat{\boldsymbol{X}}_{k+1}$, $\tilde{\boldsymbol{X}}_{k+1}$, $\hat{\boldsymbol{f}}_k$ are the estimation of $\boldsymbol{X}_{k+1}$, the state prediction of $\boldsymbol{X}_{k+1}$ and the estimation of $\boldsymbol{f}_k$, respectively. $\boldsymbol{K}_k$ is the Kalman gain matrix at time instant $t = k\Delta t$

$$\boldsymbol{K}_k = \boldsymbol{\Phi}_k\boldsymbol{P}_k\,\boldsymbol{H}_k^{\mathrm{T}}\left(\boldsymbol{H}_k\boldsymbol{P}_k\boldsymbol{H}_k^{\mathrm{T}} + \boldsymbol{R}\right)^{-1} \tag{8}$$

where

$$\boldsymbol{\Phi}_k = \boldsymbol{I} + \boldsymbol{A}_k\Delta t \tag{9}$$

$$\boldsymbol{A}_k = \frac{\partial \boldsymbol{J}(\hat{\boldsymbol{X}}_k, \boldsymbol{\theta}, \hat{\boldsymbol{f}}_k)}{\partial \hat{\boldsymbol{X}}_k} \tag{10}$$

$$\boldsymbol{H}_k = \frac{\partial \boldsymbol{h}(\hat{\boldsymbol{X}}_k, \boldsymbol{\theta})}{\partial \hat{\boldsymbol{X}}_k} \tag{11}$$

and $\boldsymbol{P}_k$ is the error covariance matrix of $\hat{\boldsymbol{X}}_k$, which can be obtained in a recursive formula as [6]

$$\boldsymbol{P}_{k+1} = \boldsymbol{\Phi}_k \boldsymbol{P}_k \boldsymbol{\Phi}_k^{\mathrm{T}} - \boldsymbol{K}_{k+1} \boldsymbol{H}_{k+1} \boldsymbol{P}_k \boldsymbol{\Phi}_k \tag{12}$$

When the measurements are available at the DOFs where the external excitations are applied, $\boldsymbol{D}$ in Eq. (4) is a non-zero matrix. The unknown external excitations $\hat{\boldsymbol{f}}_{k+1}$ can then be identified from Eq. (5) by using the least square method through the following equation

$$\hat{\boldsymbol{f}}_{k+1} = \left(\boldsymbol{D}^T \boldsymbol{D}\right)^{-1} \boldsymbol{D}^T \left\{ \boldsymbol{Y}_{k+1} - \boldsymbol{h}\left(\hat{\boldsymbol{X}}_{k+1}, \boldsymbol{\theta}\right) \right\} \tag{13}$$

2.3 System identification from subset responses

A large number of unknowns in a large structure can be divided into several smaller zones based on its finite element mesh configuration. The unknown system parameter vector $\boldsymbol{\theta}$ can be separated as several system parameter subsets $[\boldsymbol{\theta}_1, \boldsymbol{\theta}_2, \cdots, \boldsymbol{\theta}_r]$, where $\boldsymbol{\theta}_i$ contains all the unknown damage indices of the *i*-th ($1 \le i \le r$) zone. Vibration tests are conducted in the divided smaller zones with different sensor configurations and excitations are applied to obtain different sets of responses. $\ddot{\boldsymbol{x}}_{m,i}$ is the measured acceleration response vector from the sensors in the *i*-th zone, and $\boldsymbol{f}_i$ is the excitation force acting on the *i*-th zone.

The responses measured from different zones can be written as separate functions g_i of the structural parameters and excitations

$$\begin{aligned}
&\boldsymbol{g}_1(\boldsymbol{\theta}_1, \boldsymbol{\theta}_2, \cdots, \boldsymbol{\theta}_r, \boldsymbol{f}_1) - \ddot{\boldsymbol{x}}_{m,1} = 0 \\
&\boldsymbol{g}_2(\boldsymbol{\theta}_1, \boldsymbol{\theta}_2, \cdots, \boldsymbol{\theta}_r, \boldsymbol{f}_2) - \ddot{\boldsymbol{x}}_{m,2} = 0 \\
&\quad \vdots \qquad \vdots \\
&\boldsymbol{g}_i(\boldsymbol{\theta}_1, \boldsymbol{\theta}_2, \cdots, \boldsymbol{\theta}_r, \boldsymbol{f}_i) - \ddot{\boldsymbol{x}}_{m,i} = 0 \\
&\quad \vdots \qquad \vdots \\
&\boldsymbol{g}_r(\boldsymbol{\theta}_1, \boldsymbol{\theta}_2, \cdots, \boldsymbol{\theta}_r, \boldsymbol{f}_r) - \ddot{\boldsymbol{x}}_{m,r} = 0
\end{aligned} \tag{14}$$

After identifying the excitation force in the first stage, the unknowns in these functions are the damage indices of the structural parameters. The problem is to find out the solution of Eq. (14), which

can be assembled as Eq. (15)

$$\boldsymbol{G}(\boldsymbol{\theta})=0 \tag{15}$$

By using Newton method [25], we have

$$\boldsymbol{G}(\boldsymbol{\theta})=\boldsymbol{G}(\boldsymbol{\theta}^n)+\boldsymbol{G}'(\boldsymbol{\theta}^n)(\boldsymbol{\theta}^{n+1}-\boldsymbol{\theta}^n)=0 \tag{16}$$

$$\boldsymbol{G}'(\boldsymbol{\theta}^n)\boldsymbol{\theta}^{n+1}=\boldsymbol{G}'(\boldsymbol{\theta}^n)\boldsymbol{\theta}^n-\boldsymbol{G}(\boldsymbol{\theta}^n) \tag{17}$$

$$\boldsymbol{\theta}^{n+1}=\boldsymbol{\theta}^n-\left[\boldsymbol{G}'(\boldsymbol{\theta}^n)\right]^{-1}\boldsymbol{G}(\boldsymbol{\theta}^n) \tag{18}$$

where $\boldsymbol{G}'(\boldsymbol{\theta}^n)$ is the Jacobin matrix of $\boldsymbol{G}(\boldsymbol{\theta}^n)$ and can be calculated from Eq. (19).

$$\boldsymbol{G}'(\boldsymbol{\theta}^n)=\begin{bmatrix} \frac{\partial \boldsymbol{g}_1}{\partial \boldsymbol{\theta}_1} & \frac{\partial \boldsymbol{g}_1}{\partial \boldsymbol{\theta}_2} & \cdots & \frac{\partial \boldsymbol{g}_1}{\partial \boldsymbol{\theta}_r} \\ \frac{\partial \boldsymbol{g}_2}{\partial \boldsymbol{\theta}_1} & \frac{\partial \boldsymbol{g}_2}{\partial \boldsymbol{\theta}_2} & \cdots & \frac{\partial \boldsymbol{g}_2}{\partial \boldsymbol{\theta}_r} \\ \vdots & \vdots & & \vdots \\ \frac{\partial \boldsymbol{g}_r}{\partial \boldsymbol{\theta}_1} & \frac{\partial \boldsymbol{g}_r}{\partial \boldsymbol{\theta}_2} & \cdots & \frac{\partial \boldsymbol{g}_r}{\partial \boldsymbol{\theta}_r} \end{bmatrix} \tag{19}$$

2.4 Newton-SOR method

When an iterative successive over relaxation (SOR) method is used to solve Eq. (17) in each iteration, the whole process is called Newton-SOR method [24]. It could be used for solving the nonlinear systems of equations. When *l* iterations are used inside the SOR loop, it is called *l-step* Newton-SOR method. A comprehensive description of this method can be found in [24]. The SOR solution is used to reconstruct the Jacobian matrix for the next solution step so that it is not necessary to have a very high precision for the initial SOR solution [25]. Therefore, *One-step* Newton-SOR method is used in this study. For the completeness of the paper, the procedure of Newton-SOR method will be briefly described and the *One-step* Newton-SOR method will also be presented.

Eq. (17) can be written as Eq. (20) with $\boldsymbol{G}'(\boldsymbol{\theta}^n)$ decomposed as Eq. (21)

$$\left(\boldsymbol{L}-\boldsymbol{U}\right)\boldsymbol{\theta}^{n+1}=\boldsymbol{G}'(\boldsymbol{\theta}^n)\boldsymbol{\theta}^n-\boldsymbol{G}(\boldsymbol{\theta}^n) \tag{20}$$

$$\boldsymbol{G}'(\boldsymbol{\theta}^n)=\boldsymbol{L}-\boldsymbol{U} \tag{21}$$

where $\boldsymbol{L}$ is a diagonal matrix and $\boldsymbol{U}$ is a non-diagonal matrix. The right-hand-side of Eq. (20) is

defined as $\boldsymbol{b}=\boldsymbol{G}'(\boldsymbol{\theta}^n)\boldsymbol{\theta}^n-\boldsymbol{G}(\boldsymbol{\theta}^n)$. Eq. (20) can then be further written as Eqs. (22) and (23)

$$\boldsymbol{L}\boldsymbol{\theta}^{n+1}=\boldsymbol{U}\boldsymbol{\theta}^{n+1}+\boldsymbol{b} \tag{22}$$

$$\boldsymbol{L}\boldsymbol{\theta}^{n+1,l}=\boldsymbol{U}\boldsymbol{\theta}^{n+1,l-1}+\boldsymbol{b}, \qquad l=1,\ 2,\ 3\cdots \tag{23}$$

where superscript l denotes the iteration number in the SOR iteration. The solution of Eq. (22) is given in Eq. (24) by applying the SOR method

$$\boldsymbol{\theta}^{n+1,l}=\boldsymbol{L}^{-1}\left(\boldsymbol{U}\boldsymbol{\theta}^{n+1,l-1}+\boldsymbol{b}\right) \tag{24}$$

Defining $\boldsymbol{V}=\boldsymbol{L}^{-1}\boldsymbol{U}$, we have

$$\boldsymbol{V}-\boldsymbol{I}=\boldsymbol{L}^{-1}\boldsymbol{U}-\boldsymbol{I}=\boldsymbol{L}^{-1}\left(\boldsymbol{U}-\boldsymbol{L}\right) \tag{25}$$

Then Eq. (24) can be rewritten as:

$$\boldsymbol{\theta}^{n+1,l}=\boldsymbol{V}\boldsymbol{\theta}^{n+1,l-1}+\boldsymbol{L}^{-1}\boldsymbol{b} \tag{26}$$

$\boldsymbol{\theta}^{n+1,l-1}$ can be expanded similarly as Eq. (26) until $\boldsymbol{\theta}^{n+1,0}$ is reached . We then have

$$\begin{aligned}\boldsymbol{\theta}^{n+1,l}&=\boldsymbol{V}^l\boldsymbol{\theta}^{n+1,0}+\left(\boldsymbol{I}+\boldsymbol{V}+\boldsymbol{V}^2\cdots\boldsymbol{V}^{l-1}\right)\boldsymbol{L}^{-1}\boldsymbol{b}\\&=\boldsymbol{\theta}^{n+1,0}+\left(\boldsymbol{V}^l-\boldsymbol{I}\right)\boldsymbol{\theta}^{n+1,0}+\left(\boldsymbol{I}+\boldsymbol{V}+\boldsymbol{V}^2\cdots\boldsymbol{V}^{l-1}\right)\boldsymbol{L}^{-1}\boldsymbol{b}\\&=\boldsymbol{\theta}^{n+1,0}+\left(\boldsymbol{I}+\boldsymbol{V}+\boldsymbol{V}^2\cdots\boldsymbol{V}^{l-1}\right)\left(\left(\boldsymbol{V}-\boldsymbol{I}\right)\boldsymbol{\theta}^{n+1,0}+\boldsymbol{L}^{-1}\boldsymbol{b}\right)\end{aligned} \tag{27}$$

Substituting $\boldsymbol{b}=\boldsymbol{G}'(\boldsymbol{\theta}^n)\boldsymbol{\theta}^n-\boldsymbol{G}(\boldsymbol{\theta}^n)$, $\boldsymbol{V}=\boldsymbol{L}^{-1}\boldsymbol{U}$, and Eq. (21) into the last bracket of the right-hand-side of Eq. (27), we obtain

$$\begin{aligned}&\left(\boldsymbol{V}-\boldsymbol{I}\right)\boldsymbol{\theta}^{n+1,0}+\boldsymbol{L}^{-1}\boldsymbol{b}\\&\quad=\boldsymbol{L}^{-1}\left(\boldsymbol{U}-\boldsymbol{L}\right)\boldsymbol{\theta}^{n+1,0}+\boldsymbol{L}^{-1}\left(\left(\boldsymbol{L}-\boldsymbol{U}\right)\boldsymbol{\theta}^n-\boldsymbol{G}(\boldsymbol{\theta}^n)\right)\end{aligned} \tag{28}$$

Noting that the initial value and ending value in SOR iteration as $\boldsymbol{\theta}^{n+1,0}\equiv\boldsymbol{\theta}^n$ and $\boldsymbol{\theta}^{n+1,l}\equiv\boldsymbol{\theta}^{n+1}$ respectively, and substituting Eq. (28) into Eq. (27), we have

$$\boldsymbol{\theta}^{n+1}=\boldsymbol{\theta}^n-\left(\boldsymbol{I}+\boldsymbol{V}+\boldsymbol{V}^2\cdots\boldsymbol{V}^{l-1}\right)\boldsymbol{L}^{-1}\boldsymbol{G}(\boldsymbol{\theta}^n) \tag{29}$$

When $l\to\infty$, Eq. (29) is equivalent to the Newton method as presented in Eq. (18).

When $l=1$, we have the *One-step* Newton-SOR iteration as

$$\boldsymbol{\theta}^{n+1}=\boldsymbol{\theta}^n-\boldsymbol{L}^{-1}\boldsymbol{G}(\boldsymbol{\theta}^n) \tag{30}$$

With $\boldsymbol{\theta}^{n+1}$ divided as several subsets $\left[\boldsymbol{\theta}_1^{n+1},\boldsymbol{\theta}_2^{n+1},\cdots,\boldsymbol{\theta}_r^{n+1}\right]$, we have

$$\begin{bmatrix}\boldsymbol{\theta}_1^{n+1}\\ \boldsymbol{\theta}_2^{n+1}\\ \vdots\\ \boldsymbol{\theta}_r^{n+1}\end{bmatrix}=\begin{bmatrix}\boldsymbol{\theta}_1^{n}\\ \boldsymbol{\theta}_2^{n}\\ \vdots\\ \boldsymbol{\theta}_r^{n}\end{bmatrix}-\begin{bmatrix}\frac{\partial \boldsymbol{g}_1}{\partial \boldsymbol{\theta}_1^n} & 0 & 0 & 0\\ 0 & \frac{\partial \boldsymbol{g}_2}{\partial \boldsymbol{\theta}_2^n} & 0 & 0\\ 0 & 0 & \ddots & 0\\ 0 & 0 & 0 & \frac{\partial \boldsymbol{g}_r}{\partial \boldsymbol{\theta}_r^n}\end{bmatrix}^{-1}\begin{bmatrix}\boldsymbol{g}_1\left(\boldsymbol{\theta}^n,\boldsymbol{f}_1\right)-\ddot{\boldsymbol{x}}_{m,1}\\ \boldsymbol{g}_2\left(\boldsymbol{\theta}^n,\boldsymbol{f}_2\right)-\ddot{\boldsymbol{x}}_{m,2}\\ \vdots\\ \boldsymbol{g}_r\left(\boldsymbol{\theta}^n,\boldsymbol{f}_r\right)-\ddot{\boldsymbol{x}}_{m,r}\end{bmatrix} \tag{31a}$$

$$\boldsymbol{\theta}_i^{n+1}=\boldsymbol{\theta}_i^{n}-\left[\frac{\partial \boldsymbol{g}_i}{\partial \boldsymbol{\theta}_i^n}\right]^{-1}\left[\boldsymbol{g}_i\left(\boldsymbol{\theta}^n\right)-\ddot{\boldsymbol{x}}_{m,i}\right],\quad \left(i=1,2\cdots r\right) \tag{31b}$$

Tikhonov regularization technique [26] is applied to solve Eq. (31) and the solution is obtained as

$$\boldsymbol{\theta}_i^{n+1}=\boldsymbol{\theta}_i^{n}-\left[\left(\frac{\partial \boldsymbol{g}_i}{\partial \boldsymbol{\theta}_i^n}\right)^T\left(\frac{\partial \boldsymbol{g}_i}{\partial \boldsymbol{\theta}_i^n}\right)+\boldsymbol{\lambda}_i\right]^{-1}\left(\frac{\partial \boldsymbol{g}_i}{\partial \boldsymbol{\theta}_i^n}\right)^T\left[\boldsymbol{g}_i\left(\boldsymbol{\theta}^n\right)-\ddot{\boldsymbol{x}}_{m,i}\right],\left(i=1,2\cdots r\right) \tag{32}$$

After each subset parameters $\boldsymbol{\theta}_i^{n+1}$ is obtained from Eq. (32), the global structural parameters are updated iteratively and the sensitivity matrix $\boldsymbol{G}'(\boldsymbol{\theta}^{n+1})$ is re-calculated based on the updated parameters. By using Eq. (32), the parameters in each zone are updated individually. However, it should be noted that an iterative scheme will be used. The analytical responses and sensitivities in each iteration are obtained based on the global structure. Although the proposed approach is conducted based formulating the global optimization as a set of optimization problems for several smaller zones, the convergence can be achieved by using the iterative identification scheme [24].

2.5 Computational procedure of the proposed approach

The proposed approach can be applicable for both linear and nonlinear structural identification. The implementation procedure is summarized as follows:

Step 1: Divide the structure into smaller zones according to its finite element mesh configurations. Dynamic vibation tests are performed in each zone to obtain the corresponding sets of responses.

Step 2: Define the initial value of parameters as $\boldsymbol{\theta}^0=\left[\boldsymbol{\theta}_1^0,\boldsymbol{\theta}_2^0,\cdots,\boldsymbol{\theta}_r^0\right]$ based on the baseline model.

Step 3: The excitation forces in each zone of the structure $\left[\boldsymbol{f}_1,\boldsymbol{f}_2,\cdots,\boldsymbol{f}_r\right]$ can be identified from

Eqs. (6)~ (13) with the corresponding set of measurement data in each zone.

Step 4: Calculate responses of the whole structure from Eq. (1) for each test in a specific zone, and the sensitivity of responses with respect to the structural parameters of each zone $\partial \boldsymbol{g}_i / \partial \boldsymbol{\theta}_i^{n+1}$ are obtained by using Newmark-beta method [22].

Step 5: The changes in the parameters of each zone $\boldsymbol{\theta}_i^{n+1}$ can be calculated by using Eq. (32). The finite element model of the global structure is then assembled as $\boldsymbol{\theta}^{n+1} = \left[\boldsymbol{\theta}_1^{n+1}, \boldsymbol{\theta}_2^{n+1}, \cdots, \boldsymbol{\theta}_r^{n+1}\right]$.

Step 6: Repeat Steps 3–5 until the convergence criterion in Eq. (33) is met.

$$\frac{\left\|\boldsymbol{\theta}^{n+1} - \boldsymbol{\theta}^{n}\right\|}{\left\|\boldsymbol{\theta}^{n+1}\right\|} \times 100\% \le \boldsymbol{Tol} \tag{33}$$

where ***Tol*** is the defined d tolerance value, which will be given in the following numerical and experimental studies.

Repeated vibration tests with a limited number of sensors can be conducted in all divided zones separately so as to reduce the required number of sensors and channels for the updating of the target zones when a substructural strategy is used, and the computational load consumed in updating the global large-scale structures. Only the measured responses are used for identification. These are the main merits of the proposed approach. However, like many output only damage detection methods [4, 6, 11, 14], the proposed approach requires that: a) the number of the measured responses is larger than that of the unknown excitations; and b) the responses at the locations of the applied excitations in each zone shall be available. These two conditions can be satisfied for engineering applications, for example, when using impact hammer, shakers or drop-weight impact machines for the dynamic tests in each zone, the information regarding the locations of these applied excitations is usually available and the number of placed sensors shall be larger than the number of a few excitation forces.

3 Numerical Studies

To validate the effectiveness and accuracy of the proposed approach for system identification of linear and nonlinear structures, numerical studies on a nonlinear multi-story shear frame and a planar steel truss are conducted. Only measured responses are used for the identification of the external

excitation and structural parameters.

3.1 System identification of a 6-DOF nonlinear structure

Considering a six-storey nonlinear elastic Duffing-type shear building subjected to a ground motion acceleration $\ddot{x}_g(t)$, the system equation of motion is given by [5, 23]

$$m_i\left(\sum_{j=1}^{i}\ddot{x}_i(t)\right)+c_i\dot{x}_i(t)-c_{i+1}\dot{x}_{i+1}(t)+k_i x_i(t) - k_{i+1}x_{i+1}(t)+K_i x_i^3(t)-K_{i+1}x_{i+1}^3(t)=m_i\ddot{x}_g(t) \quad (i=1,2,3,4,5) \quad (34a)$$

$$m_i\left(\sum_{j=1}^{i}\ddot{x}_i(t)\right)+c_i\dot{x}_i(t)+k_i x_i(t)+K_i x_i^3(t)=m_i\ddot{x}_g(t), \quad (i=6) \quad (34b)$$

in which x_i is the inter-storey drift displacement between the i-th and (i+1)-th stories (i=1~5), $m_1=m_2=\cdots=m_6=600kg$, $c_1=c_2=\cdots=c_6=1kNs/m$, $k_1=k_2=\cdots=k_5=1.2\times10^5 N/m$, $k_6=0.6\times10^5 N/m$, $K_1=K_2=\cdots=K_5=2\times10^8 N/m^3$, and $K_6=10^8 N/m^3$. The applied ground motion is simulated based on a similar procedure in a previous study [27] and generated as a white noise acceleration history, which is then scaled to have a maximum peak ground acceleration (PGA) of 0.3g and low pass filtered with a frequency range from 0-20Hz. This relatively small ground motion is applied to ensure the structure behaves linearly. For the elastic structure with no nonlinear terms, that is $K_1=K_2=\cdots=K_6=0$, the first three natural frequencies are $\omega_1=0.538$Hz, $\omega_2=1.473$Hz and $\omega_3=2.251$Hz.

Sensors are installed at each floor to measure the accelerations with a sampling frequency of 2000Hz. In this example, the masses (m_1, m_2,⋯, m_6), damping (c_1, c_2, ⋯, c_6) and stiffness (k_1, k_2,⋯, k_6) are assumed known. The parameters of the nonlinear Duffing model (K_1, K_2,⋯, K_6) and the input ground motion $\ddot{x}_g(t)$ are unknowns to be identified. Based on the proposed approach, the Kalman filter technique is used to identify the excitation force, and the system parameters are updated with the Newton-SOR method.

The shear building structure is divided into two zones, namely, a lower level structure and an upper-level structure, as shown in Figure 1. The first zone consists of unknown parameters

($\boldsymbol{\theta}_1 = [K_1,\ K_2,\ K_3]$) and the second zone consists of unknown parameters ($\boldsymbol{\theta}_2 = [K_4,\ K_5,\ K_6]$). There are respectively three accelerometers in each zone to measure the vibration responses. The response data collected in the first second are used for the identification. The convergence criterion in Eq. (33) is set equal to 10^{-6} for the case without noise and 10^{-3} for the case with noise. The initial value of unknown parameters are defined as $K_1 = K_2 = \cdots = K_5 = 2.4\times10^8 N/m^3$ and $K_6 = 1.2\times10^8 N/m^3$.

Firstly, the unpolluted acceleration responses are used to verify the accuracy of the proposed approach for the identification of nonlinear system parameters. Figure 2 shows the identified results with iterations when responses without smeared with noise are used for identification. The identified ground motion as shown in Figure 3 matches well with the true ground motion. The relative error in the ground motion identification is 0.115%. These results show that the proposed approach can identify the system parameters and unknown ground motion simultaneously with a very good accuracy.

To study the noise effect in the measurements on the identification accuracy, the noisy response is simulated by adding a random white noise to the original analytical response as

$$\ddot{\boldsymbol{x}}_m = \ddot{\boldsymbol{x}} + E_p \boldsymbol{N}_{noise}\sigma(\ddot{x}) \tag{35}$$

where E_p is percentage of the noise level, $\boldsymbol{N}_{noise}$ is a standard normal distribution vector with zero mean and unit standard deviation, $\sigma(\ddot{x})$ is the standard deviation of the original analytical acceleration response. 5% and 10% noise levels are considered in this study. The 4th-order Butterworth band-pass filter of a frequency range from 0.1~100 Hz is used to pre-process the signals and remove the high frequency noise.

The identified nonlinear system parameters with measurement noises are shown in Figure 4. The maximum identified error for 5% noise case is 4.25% at the floor 6, while the maximum identified error for 10% noise case is 5.63% at the floor 3. The other identification errors are small. The comparison between the identified and true ground motions is shown in Figure 5. The relative errors are 1.45% and 3.49% between the true and identified ground motions for the 5% and 10% noise cases, respectively. These results demonstrate that the proposed approach can well identify the nonlinear system parameters and the excitation force even under a significant measurement noise effect.

3.2 System identification of a linear plane truss structure

A simply-supported plane truss structure used in a previous work [22] is selected for conducting a comparison study. The dimensions are shown in Figure 6. The structure is modeled with forty-six planar truss finite elements. The finite element model has 40 degrees-of-freedom. The cross-sectional area of the bar is 0.0016 m^2. The first eight natural frequencies of the structure are 0.73, 2.02, 2.86, 5.05, 6.51, 7.77, 9.91 and 10.49 Hz respectively. Rayleigh damping with ξ_1=0.01 and ξ_2=0.01 is assumed as the damping ratios of the first two modes. The mass density is 7.8×10^3 kg/m^3, and the elastic modulus is 206 GPa. The truss is pin-supported at Node 1 and roller-supported at Node 18. The restraints at the supports are represented by a large stiffness of 10^8 kN/m.

3.2.1 Force identification

The proposed approach requires to identify the unknown input force and structural parameters at each iteration. Since the accuracy of the force identification results would affect the accuracy of damage identification, the accuracy of force identification with different settings is studied in this section. To investigate the selection of different sampling rates and covariance matrices on the force identification accuracy, taking zone 2 as an example, structural parameters are assumed as known and only the force on Node 10 is considered as unknown.

The sensor layout is shown in Figure 7(b). The effect of different sampling rates and covariance matrices on the force identification is studied. Table 1 shows the errors in the force identification results with four different sampling rates from 500Hz to 5000Hz and three covariance matrices in Kalman filter. Since the structure is at rest before the application of external force, the value of $\hat{\boldsymbol{X}}_0$ in Eq. (6) is selected as zero for all studies.

The identification results listed in Table 1 indicate that the sampling rate may significantly affect the accuracy of force identification, however, the definition of covariance matrix of measurement noise may not. The error in the identified force increases when the sampling rate decreases because the responses with a higher sampling rate consist of more information. Based on this parametric study and considering the balance between the computational load and identification accuracy, the sampling rate and the covariance matrix are defined as 2000Hz and $0.01\times\boldsymbol{I}$, respectively.

3.2.2 Decentralized structural identification

The truss structure is arbitrarily divided into three zones. The first zone, second zone and third zone consist of members 1 to 15 with unknown elemental stiffness parameters $\alpha_1 \sim \alpha_{15}$, members 16 to 30 with unknown elemental stiffness parameters $\alpha_{16} \sim \alpha_{31}$ and members 31 to 46 with unknown parameters $\alpha_{32} \sim \alpha_{46}$. The placed accelerometers for measuring the vibration responses in each zone are shown in Figure 7. Vibration measurements in a specific zone are only used for the identification of excitation forces and stiffness parameters associated with this zone. The input force is a band pass ambient force with a bandwidth of 0-400Hz and a standard deviation of 40 N. The sampling rate is 2000 Hz and 1 second vibration data are used for the identification. 10%, 20% and 15% stiffness reductions are assumed in elements 8, 24 and 38, respectively.

Acceleration responses with and without noise effect from the damaged structures are used. Figure 8 shows the identification results for different subsets of structural parameters in all the three zones when measurements without noise effect are used for the identification. The locations and severities of the preset three damages in different zones can be accurately identified. Small identification errors (less than 2%) are observed in other undamaged elements. This may be caused by the numerical errors in the proposed algorithm. Figure 9 shows the comparison of true and identified excitation forces without noise effect. The identified force matches well with the true one with a relative error of 0.0434%. When noisy responses are used for identification, the fourth-order Butterworth band-pass filter with a frequency range from 0.1 to 500 Hz is used to remove the high frequency noise. The identified stiffness reduction factors with different levels of measurement noise are shown in Figure 10. Both damage locations and severities in different zones are well identified. The maximum identified error for the 5% noise case is 5.31% at element 5 and the other errors are less than 5%. There are two large identified errors, that is, 6.53% at element 19 and 8.71% at Element 20, for 10% noise case. The identified forces are compared with the true force in Zone 2 and shown in Figure 11. The relative errors in the force identification are 14.43% and 23.16% for the 5% noise case and 10% noise case, respectively. The identified excitation forces generally show a good agreement with the true force, even the recorded data are polluted with noise. These results demonstrate that the proposed approach can accurately identify the structural damage and external force when no noise responses are used. The identification is also good when significant measurement

noise effect is considered.

It should be noted that in the previous work [22], it took about 3 hours for the model updating. However, the proposed approach only needs less than 5 mins with the same simulation data since only the unknown parameters in a smaller zone are involved in the sensitivity based identification. Two advantages of the improved approach has been demonstrated through the numerical studies: 1) It can be used for both linear and nonlinear system identification with output only; 2) It takes less computational time compared with the previous method.

4 Experimental Verifications

Experimental verifications on an eight-story shear-type steel frame model are conducted to validate the proposed decentralized system identification approach. Figure 12 shows the testing model in the laboratory. The height and width of steel structure are 2000 mm and 600 mm, respectively. The floor of each story is constructed by thick steel plates (100 mm×25mm), and the two columns of each story have the same cross section with a width of 50 mm and a thickness of 5 mm. The beams and columns are welded to form rigid joints. The bottom of two columns is welded onto a thick and solid steel plate, which is fixed to the strong floor. The dimensions of the frame model are shown in Figure 13. The initial elastic modulus of the steel is estimated as 200 GPa, and the mass density 7850 kg/m^3.

4.1 Experimental setup and initial model updating

An SINOCERA LC-04A hammer with a rubber tip is used to apply the excitation on the model. KD1300 accelerometers are installed at all the floors to measure horizontal acceleration responses. A commercial data logging system INV306U and its associated signal analysis package DASP V10 are used for data acquisition. The initial shear-type building finite element model is built based on the dimensions and material properties of the frame. An evitable discrepancy between the numerical finite element model and experimental model exist due to the modelling errors and uncertainties in the material properties and boundary conditions. Vibration testing data from the experimental model under the healthy state are used to perform an initial model updating to minimize the difference between the experimental and analytical models.

Vibration tests are performed by using the hammer to hit on the frame model in different divided zones. Both applied force from the hammer and accelerations are recorded for 60s. Only the first 0.5

second data are selected for damage detection. The sampling rate is set as 1024 Hz, and the cut-off frequency range for the band-pass filter is defined from 1Hz to 100Hz for all tests. The finite element model of the shear frame is divided into two zones. The first zone consists of 1-4 floors, and the second zone 5-8 floors. For the first vibration test, sensors are installed in the first zone from 1-4 floors to measure the horizontal acceleration responses when subjected to a hammer impact force at the third floor. For the second test, sensors are installed in the second zone from 5-8 floors to measure the vibration responses with the impact located at the 7th floor. Only the structural stiffness parameters and excitation forces are updated with the proposed approach. The measured and analytcial natural frequencies of the experimental model before and after model updating are listed in Table 2. The maximum error in the frequencies after updating is only 0.26%. The measured and analytical mode shapes of the model are shown in Figure 14. The mode shapes after model updating match very well with the measured mode shapes from the vibration tests. These indicate that an accurate initial finite element model is achieved to serve as the baseline model in the subsequent studies on structural identification.

4.2 Decentralized system identification

Damages are introduced by reducing the cross section of the column of the frame model. Two damage cases, i.e. case 1 and case 2, are introduced. Only a single damage is introduced in case 1 with 40% cross section reduction of a column of the 2nd floor of the frame model. This will produce 20% reduction to the equivalent stiffness of the 2nd floor. Case 2 has multiple damages. Besides the damage in case 1, another damage is introduced with 20% cross section of a column at the 7th floor of the frame model. This is equivalent to 10% stiffness reduction in the 7th floor. Those introduced damages in the second and seventh floors are shown in Figure 15.

The frame is tested with the same sensor placement and definition of zones as described in Section 4.1. The reduction of the mass caused by the damage is neglected. Measured responses are used to identify the structure damages and applied excitation force. The updated numerical model obtained in Section 4.1 is used as the baseline model. The identification results for those two cases are shown in Figure 16. In case 1, the identified damage in the second floor is 19%, which is very close to the true value of 20%. For case 2, the identified stiffness reductions are 19.8% at floor 2 and 10.4% at floor 7. It can be observed from the identification results of those two cases, both damage locations and severities can be well identified with the proposed approach. However, it should be noted that some errors, i.e. around 4% false identified stiffness reductions are observed in the 3rd floor to the 6th floor. The identified forces have a good agreement with the measured forces, i.e. the force

applied in Zone 2 in case 2, as shown in Figure 17. The relative error in the force identification is 35.57% which is larger than that in numerical studies. These errors in identified excitation force and stiffness parameters are due to the noise effect in measurements and uncertainty effect in finite element model and experimental tests. The above results in experimental verifications demonstrate that the proposed approach well identify the structural damage and applied excitation force.

5 Conclusions

This paper proposes an improved decentralized system identification approach for both linear and nonlinear structures with output measurements only. The proposed approach divides a large scale structure into several zones for identification. Kalman filter technique is used to identify the unknown input force, and Newton-SOR method is adopted for identifying the unknown structural parameters. The external excitations and structural parameters are updated iteratively. Numerical studies on a six-floor nonlinear system and a linear planar truss structure demonstrate that the proposed approach is effective for output−only structural identification with a few sensors even when 10% noise effect is included in the measured data. An experimental eight-story shear-type steel frame structure was also tested in the laboratory to validate the proposed approach. Two damage cases were introduced in the model. The applied excitation force and structure damage in both the damage cases are well identified with the measured responses. It is demonstrated that the proposed approach can be used for both linear and nonlinear system identification by using only measured responses, and needs less number of measurement sensors, and less computational time compared with the existing methods. More experimental investigations on using the proposed approach for the identification of nonlinear structures shall be conducted in the future to further demonstrate its effectiveness.

Acknowledgements

The work described in this paper was supported by the National Research Foundation of Korea (NRF) grant funded by the Korea government (MSIP) through GCRC-SOP (No. 2011-0030013) and an ARC Linkage project LP160100528.

References

[1] J. Li, J. Chen, A statistical average algorithm for the dynamic compound inverse problem, Computational Mechanics, 30 (2003) 88-95.

[2] Z.R. Lu, S.S. Law, Identification of system parameters and input force from output only, Mechanical Systems and Signal Processing, 21 (2007) 2099-2111.

[3] H. Huang, J.N. Yang, L. Zhou, Adaptive quadratic sum‐squares error with unknown inputs for damage identification of structures, Structural Control and Health Monitoring, 17 (2010) 404-426.

[4] J.N. Yang, H. Huang, Sequential non-linear least-square estimation for damage identification of structures with unknown inputs and unknown outputs, International Journal of Non-Linear Mechanics, 42 (2007) 789-801.

[5] J.N. Yang, S. Lin, H. Huang, L. Zhou, An adaptive extended Kalman filter for structural damage identification, Structural Control and Health Monitoring, 13 (2006) 849-867.

[6] Y. Lei, Y. Wu, T. Li, Identification of non-linear structural parameters under limited input and output measurements, International Journal of Non-Linear Mechanics, 47 (2012) 1141-1146.

[7] M. Wu, A.W. Smyth, Application of the unscented Kalman filter for real-time nonlinear structural system identification, Structural Control and Health Monitoring, 14 (2007) 971-990.

[8] Z. Xie, J. Feng, Real-time nonlinear structural system identification via iterated unscented Kalman filter, Mechanical Systems and Signal Processing, 28 (2012) 309-322.

[9] S. Weng, Y. Xia, X.Q. Zhou, Y.L. Xu, H.P. Zhu, Inverse substructure method for model updating of structures, Journal of Sound and Vibration, 331 (2012) 5449-5468.

[10] S. Weng, H.P. Zhu, Y. Xia, L. Mao, Damage detection using the eigenparameter decomposition of substructural flexibility matrix, Mechanical Systems and Signal Processing, 34 (2013) 19-38.

[11] C.G. Koh, B. Hong, C.Y. Liaw, Substructural and progressive structural identification methods, Engineering Structures, 25 (2003) 1551-1563.

[12] K.V. Yuen, L.S. Katafygiotis, Substructure identification and health monitoring using noisy response measurements only, Computer‐Aided Civil and Infrastructure Engineering, 21 (2006) 280-291.

[13] S.S. Law, K. Zhang, Z.D. Duan, Structural damage detection from coupling forces between substructures under support excitation, Engineering Structures, 32 (2010) 2221-2228.

[14] Y. Lei, C. Liu, Y. Jiang, Y. Mao, Substructure based structural damage detection with limited input and output measurements, Smart Structures and Systems, 12 (2013) 619-640.

[15] C. Koh, K. Shankar, Substructural identification method without interface measurement, Journal of Engineering Mechanics, 129 (2003) 769-776.

[16] J. Li, S. Law, Substructural damage detection with incomplete information of the structure, Journal of Applied Mechanics, 79 (2012) 041003.

[17] J. Li, H. Hao, Substructure damage identification based on wavelet-domain response reconstruction, Structural Health Monitoring, 13 (2014) 389-405.

[18] S.-H. Sim, B. Spencer, M. Zhang, H. Xie, Automated decentralized modal analysis using smart sensors, Structural Control and Health Monitoring, 17 (2010) 872-894.

[19] H. Jo, S.-H. Sim, T. Nagayama, B. Spencer Jr, Development and application of high-sensitivity wireless smart sensors for decentralized stochastic modal identification, Journal of Engineering Mechanics, 138 (2011) 683-694.

[20] Z. Wu, B. Xu, K. Yokoyama, Decentralized parametric damage detection based on neural networks, Computer‐Aided Civil and Infrastructure Engineering, 17 (2002) 175-184.

[21] G.J. Yun, S.-G. Lee, J. Carletta, T. Nagayama, Decentralized damage identification using wavelet signal analysis embedded on wireless smart sensors, Engineering Structures, 33 (2011) 2162-2172.
[22] S.S. Law, P.H. Ni, J. Li, Parallel Decentralized Damage Detection of a Structure with Subsets of Parameters, Aiaa Journal, 52 (2014) 650-656.
[23] J.N. Yang, S. Pan, H. Huang, An adaptive extended Kalman filter for structural damage identifications II: unknown inputs, Structural Control and Health Monitoring, 14 (2007) 497-521.
[24] J.M. Ortega, W.C. Rheinboldt, Iterative solution of nonlinear equations in several variables, Siam, 1970.
[25] G. Carey, R. Krishnan, On a nonlinear iterative method in applied mechanics, part II, Computer Methods in Applied Mechanics and Engineering, 30 (1982) 323-333.
[26] A.N. Tikhonov, A. Goncharsky, V. Stepanov, A.G. Yagola, Numerical methods for the solution of ill-posed problems, Springer Science & Business Media, 2013.
[27] Y. Xu, J. Zhang, J. Li, Y. Xia, Experimental investigation on statistical moment-based structural damage detection method, Structural Health Monitoring, 8 (2009) 555-571.

Table 1. Identification results with different sampling rates and covariance matrices

Sampling frequency (Hz)	Covariance matrix $\boldsymbol{R}$		
	$\boldsymbol{I}$	$0.01\times\boldsymbol{I}$	$0.001\times\boldsymbol{I}$
500	7.74%	7.32%	6.49%
1000	2.45%	2.21%	2.49%
2000	0.73%	0.74%	1.22%
5000	0.34%	0.18%	0.17%

Note: $\boldsymbol{I}$ is an identity matrix

Table 2. Measured and analytical natural frequencies of the experimental model before and after updating

Mode	Tested	Before updating		After updating	
		Analytical (Hz)	Error (%)	Analytical (Hz)	Error (%)
1	4.645	4.810	-3.552	4.636	-0.1905
2	13.705	14.267	-4.101	13.714	0.0635
3	22.554	23.238	-3.033	22.558	0.0156
4	30.695	31.418	-2.355	30.776	0.2649
5	38.241	38.528	-0.7505	38.225	-0.0426
6	44.434	44.325	0.245	44.422	-0.0269
7	48.826	48.614	0.434	48.712	-0.2343
8	52.306	51.246	2.027	52.161	-0.2771

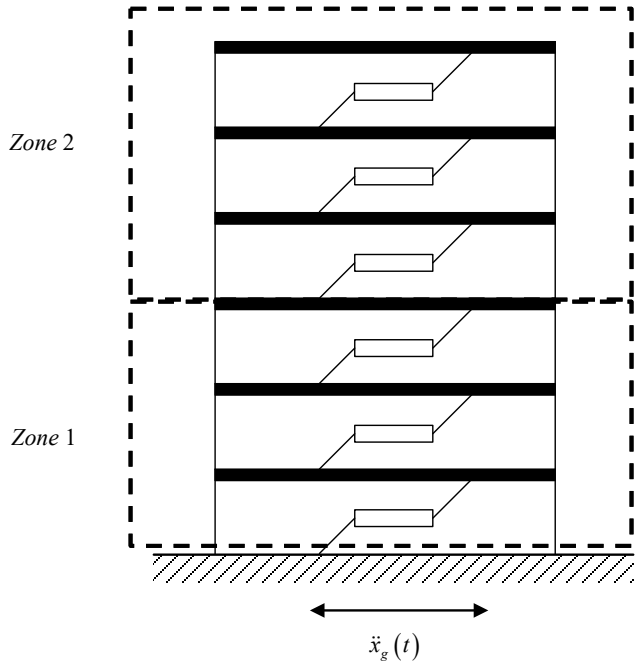

Figure 1. The nonlinear shear building model in the numerical study

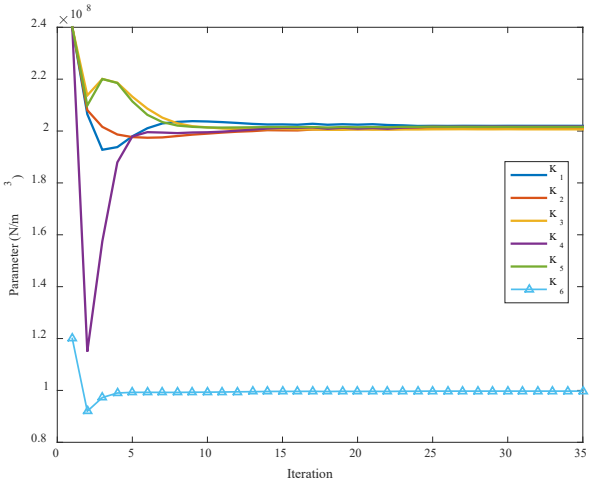

Figure 2. Identified system parameters with iterations

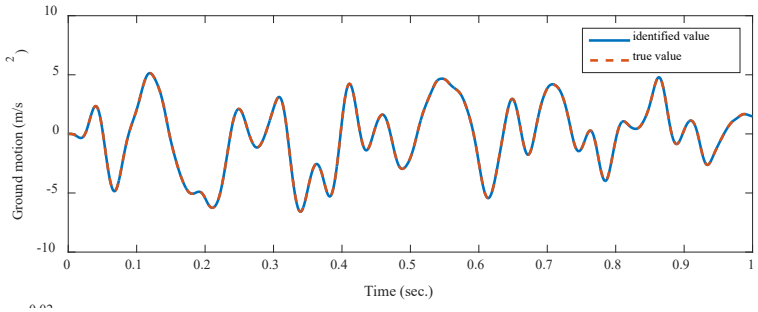

Figure 3. Identified ground motion without noise effect

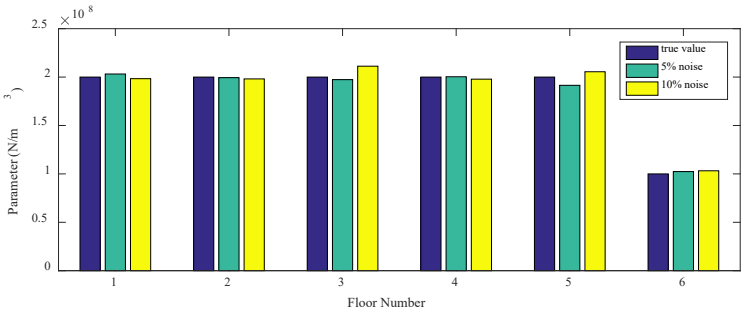

Figure 4. Identified system parameters with noise effect

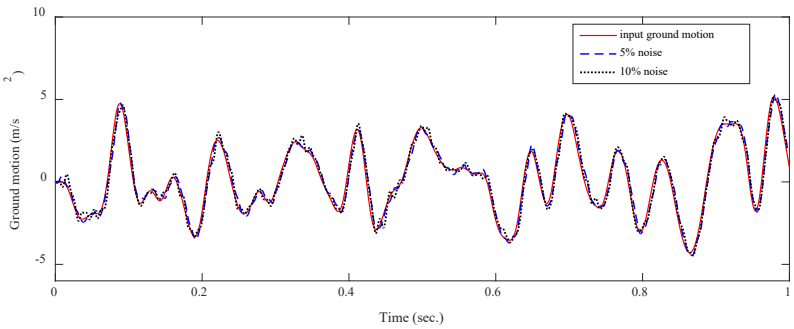

Figure 5. Identified ground motion with noise effect

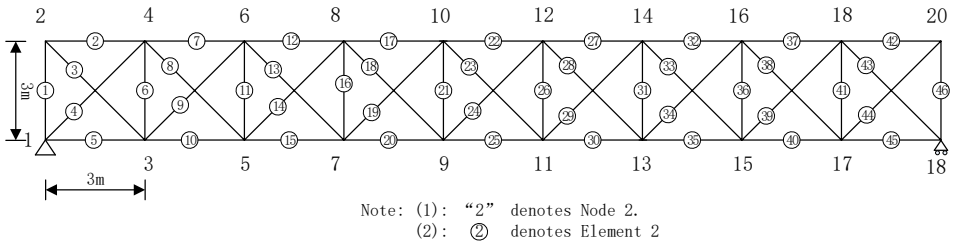

Figure 6. A linear truss structure model in the numerical study

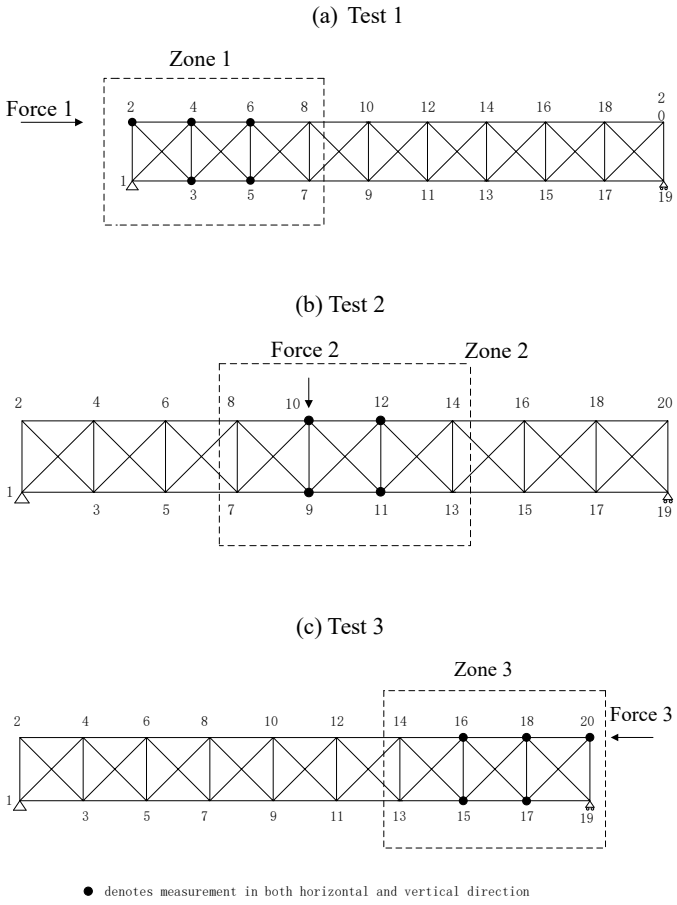

Figure 7. The sensor placements in divided zones of the truss model

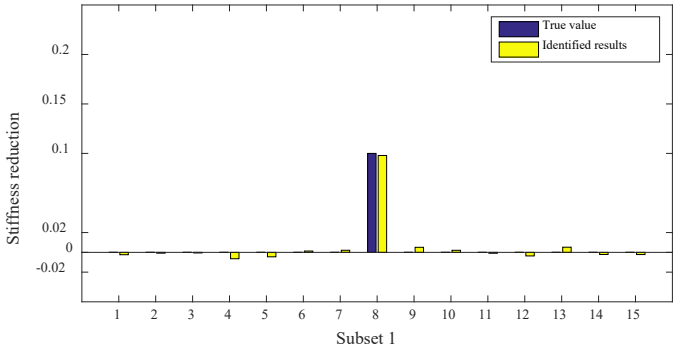

1) Zone 1

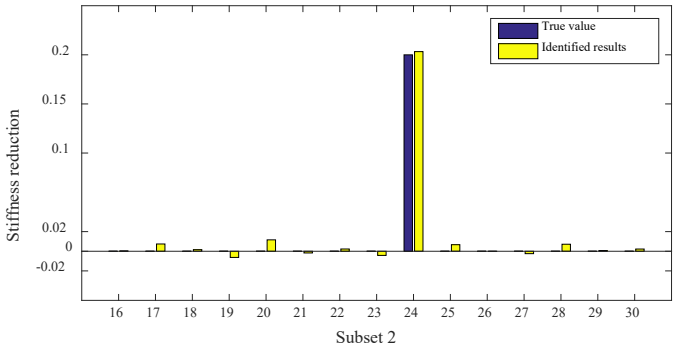

2) Zone 2

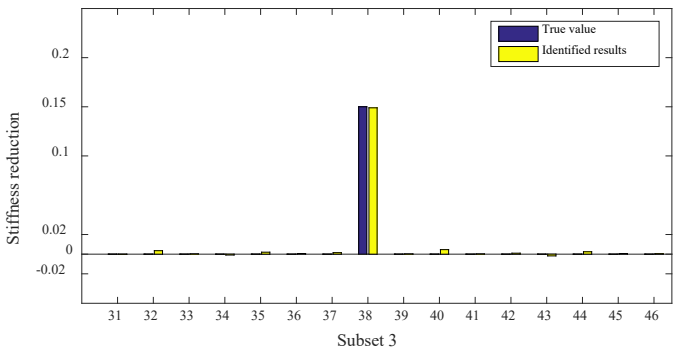

3) Zone 3

Figure 8. Damage identification results without noise effect

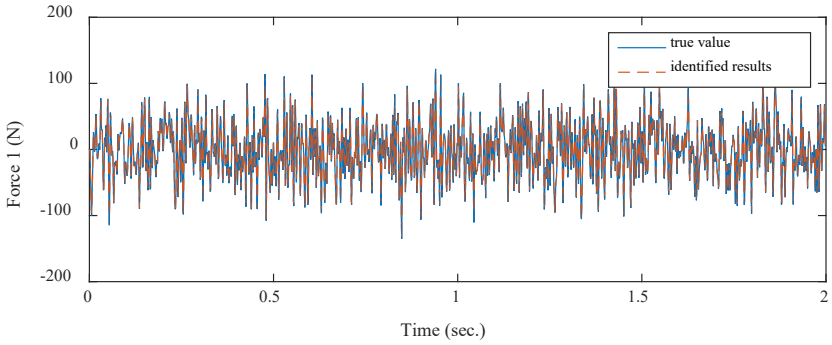

(a) True and identified forces in Zone 1

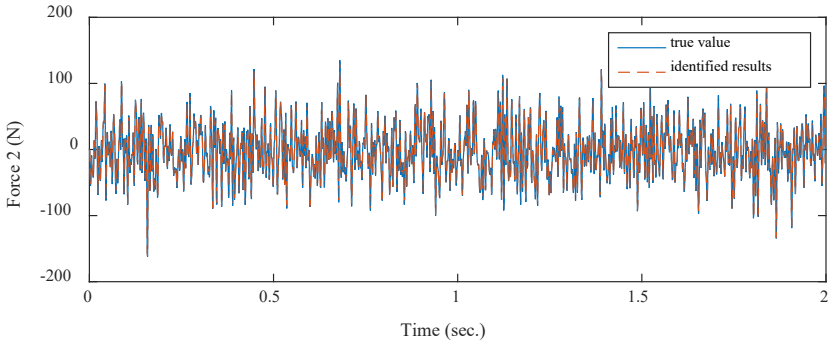

(b) True and identified forces in Zone 2

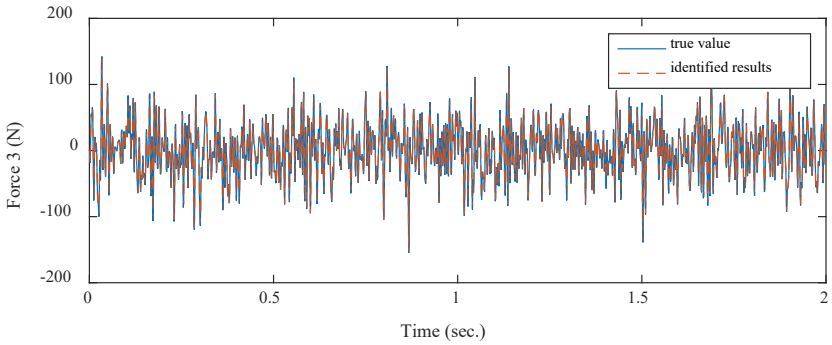

(c) True and identified forces in Zone 3

Figure 9. The comparison between the identified and true forces without measurement noise

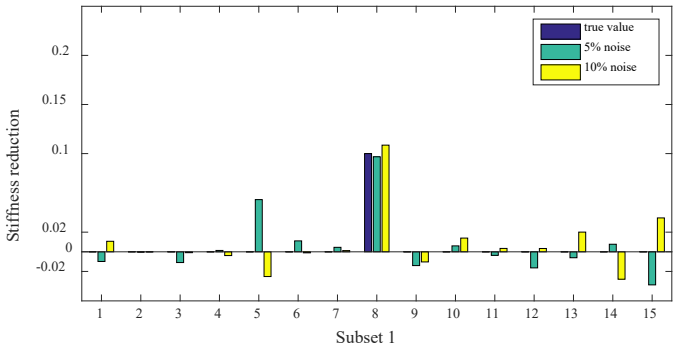

(a) Zone 1

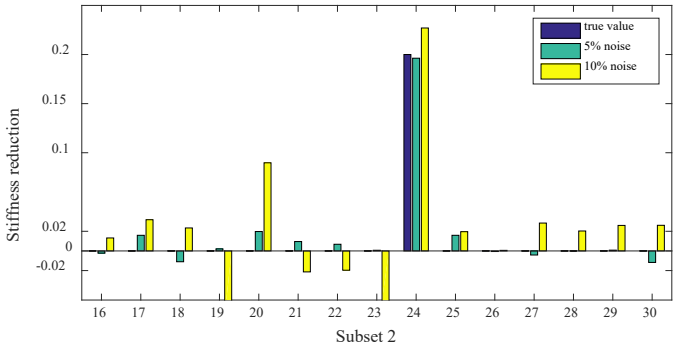

(b) Zone 2

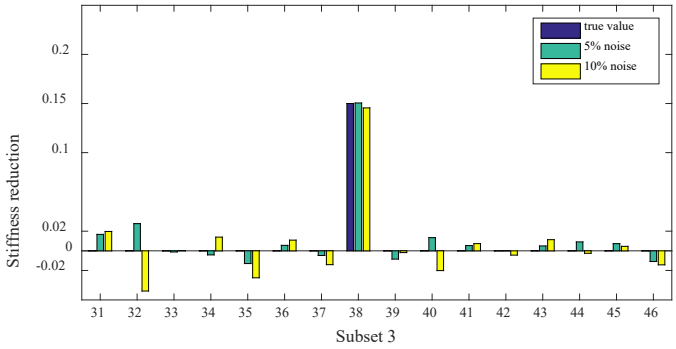

(c) Zone 3

Figure 10. Damage identification results with different noise levels

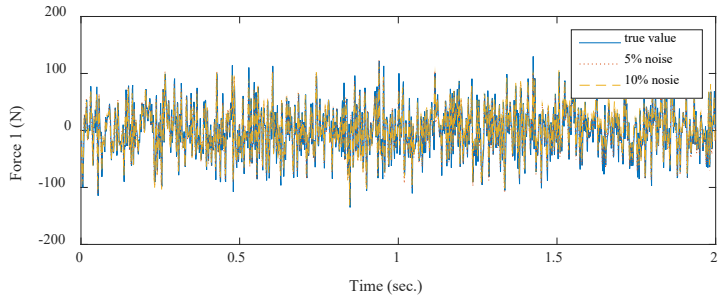

(a) Identified force in zone 1

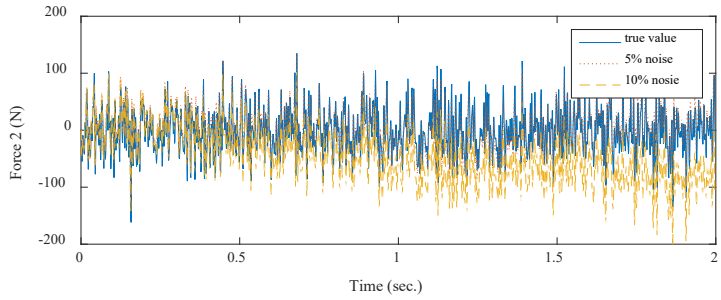

(b) Identified force in zone 2

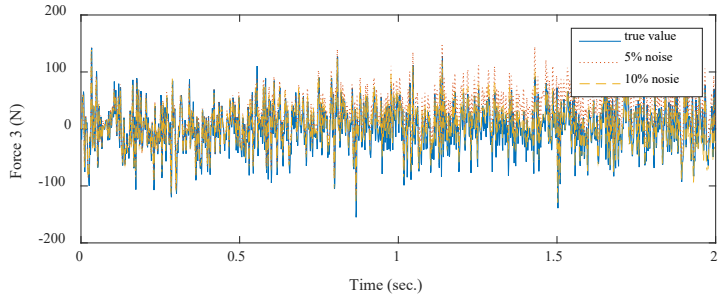

(c) Identified force in zone 3

Figure 11. The comparison between the identified and true forces with different noise levels in the measurements

Figure 12. Laboratory steel frame model

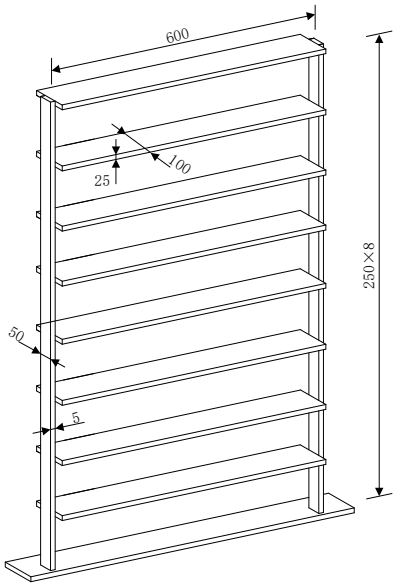

Figure 13. Dimensions of the steel frame model (unit: mm)

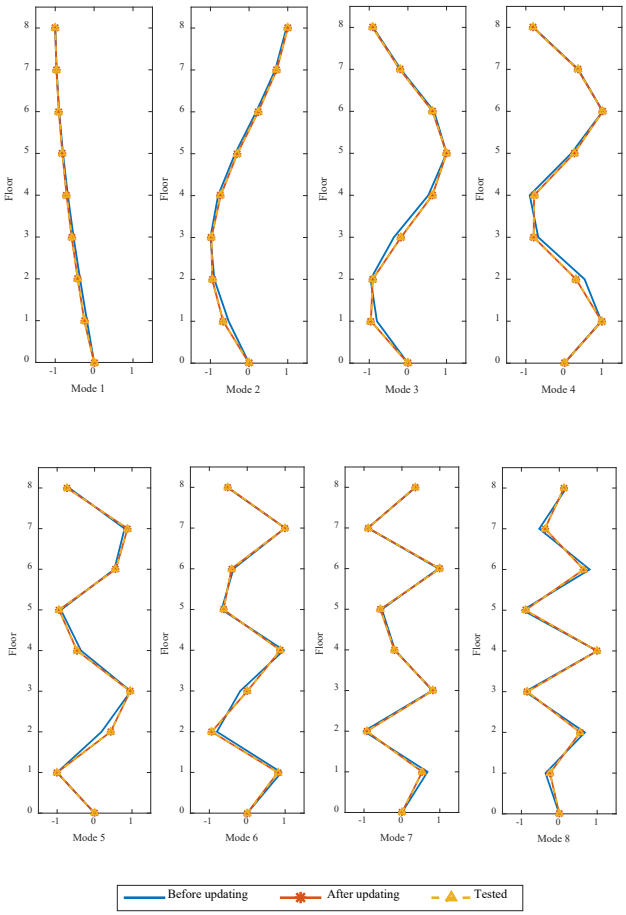

Figure 14. Mode shapes before and after updating

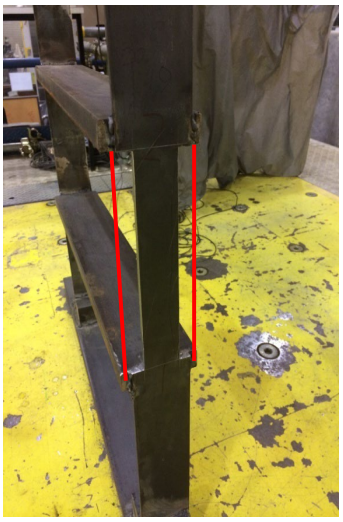

(a) Introduced damage at the 2nd floor (40% reduction of cross section area of one column)

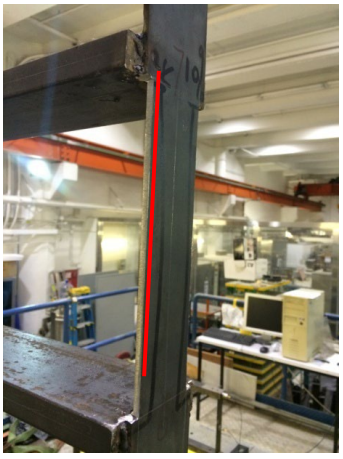

(b) Introduced damage at the 7th floor (20% reduction of cross section area of one column)

Figure 15. Introduced damages of the frame model

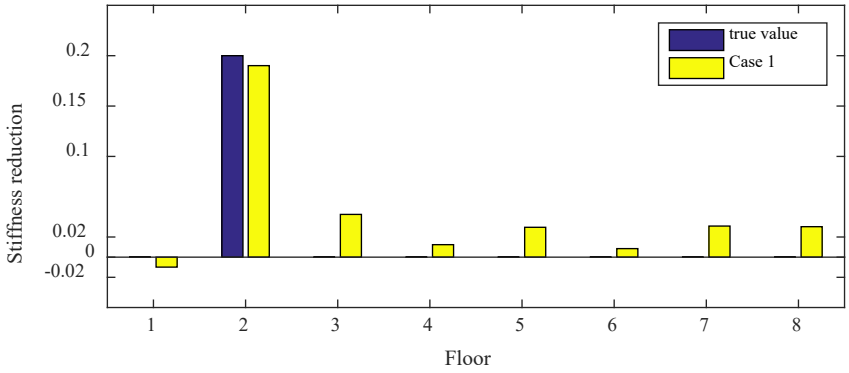

(a) Identified results of case 1

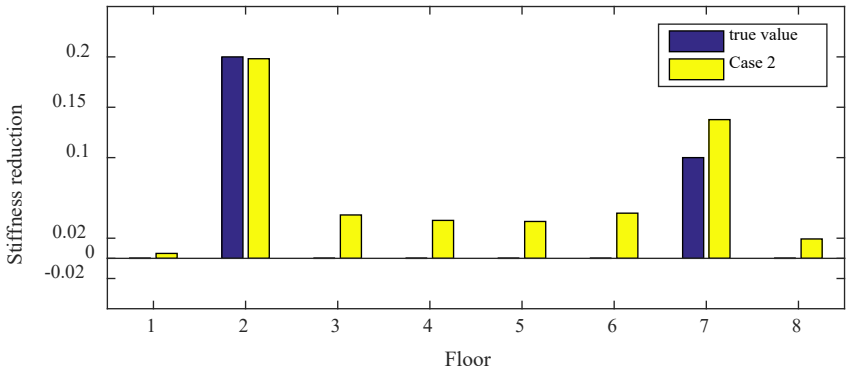

(b) Identified results of case 2

Figure 16. Damage identification results in experimental studies

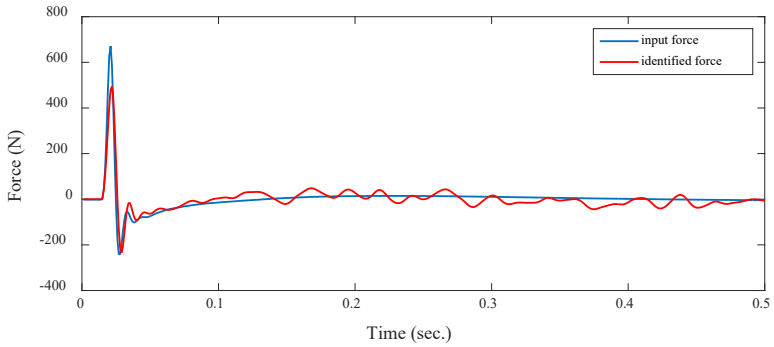

Figure 17. Comparison of true and identified force in Zone 2 (Case 2)